Supplementary Information

Anthropogenic Effects on Tropical Cyclones near Western Europe

Shuai Wang[1], Hiroyuki Murakami[2], and William Cooke[2]

[1] Department of Geography and Spatial Sciences, University of Delaware, DE, USA
[2] National Oceanic and Atmospheric Administration/Geophysical Fluid Dynamics Laboratory, Princeton, NJ, USA
* Corresponding author: Shuai Wang, shwang@udel.edu

This file contains:

Supplementary Tables 1 and 2
Supplementary Figures 1-11

Supplementary Table 1. Coefficient of determination (r^2) values, showing the relationship between the expansion coefficient for SST of the first and second global SVD modes (EC_SST mode 1 and EC_SST mode 2) and various climatic indices: the Interdecadal Pacific Oscillation (IPO), El Niño-Southern Oscillation (ENSO), Atlantic Meridional Oscillation (AMO), Atlantic Meridional Mode (AMM) and the global mean SST time series (MEAN_SST), over the period from 1960 to 2020. Bold numbers indicate statistical significance at a 5% level, determined using the two-sided Wald Test with a *t*-distribution for the test statistic.

	IPO	ENSO	AMO	AMM	MEAN_SST
EC_SST (mode 1)	0.05	0.03	**0.61**	**0.18**	**0.84**
EC_SST (mode 2)	**0.74**	**0.71**	**0.08**	<0.01	**0.36**

Supplementary Table 2. Decomposition of ENGPI trend. The ENGPI equation is linearized by taking the logarithm. The mean log(ENGPI) change in the main development region is broken down into the relative contribution (in a unit of %) of four terms related to the change of absolute vorticity (VORT), relative humidity (RH), potential intensify (MPI), and vertical wind shear (V-SHEAR). A positive contribution of one term means the logarithm of the trend of this term shows the same sign as the mean log(ENGPI) trend difference.

	VORT	RH	MPI	V-SHEAR	Total contribution
Aerosol effect (1966-2020)	20%	48%	4%	28%	100%
GHG effect (2030-2100)	22%	38%	9%	31%	100%

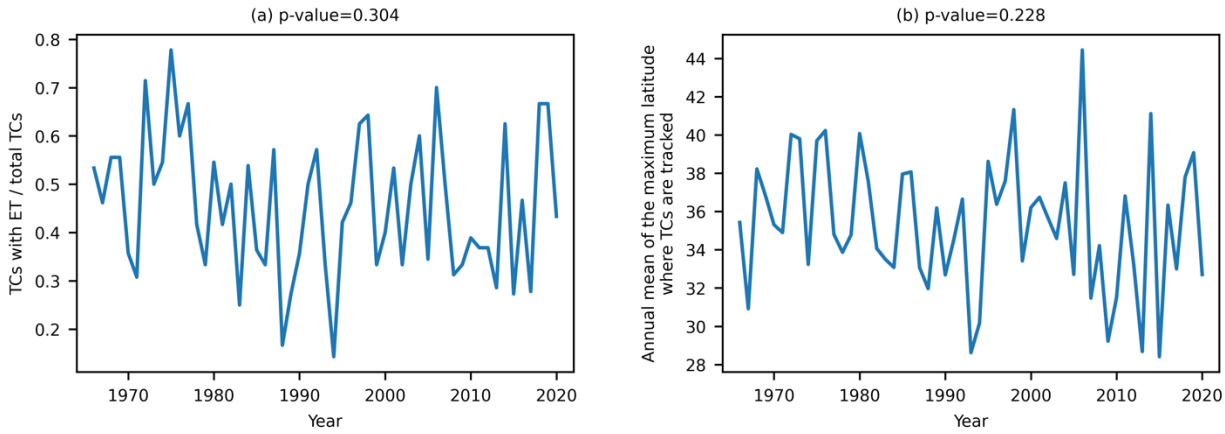

Supplementary Figure 1. Time series of (a) the annual ratio of count of TCs with extratropical transition to the total TC number, and (b) the annual mean of the maximum latitudes recorded of each TC in a year. The *p*-value in the title was calculated from a hypothesis test whose null hypothesis is that the slope is zero by Wald Test with *t*-distribution of the test statistic.

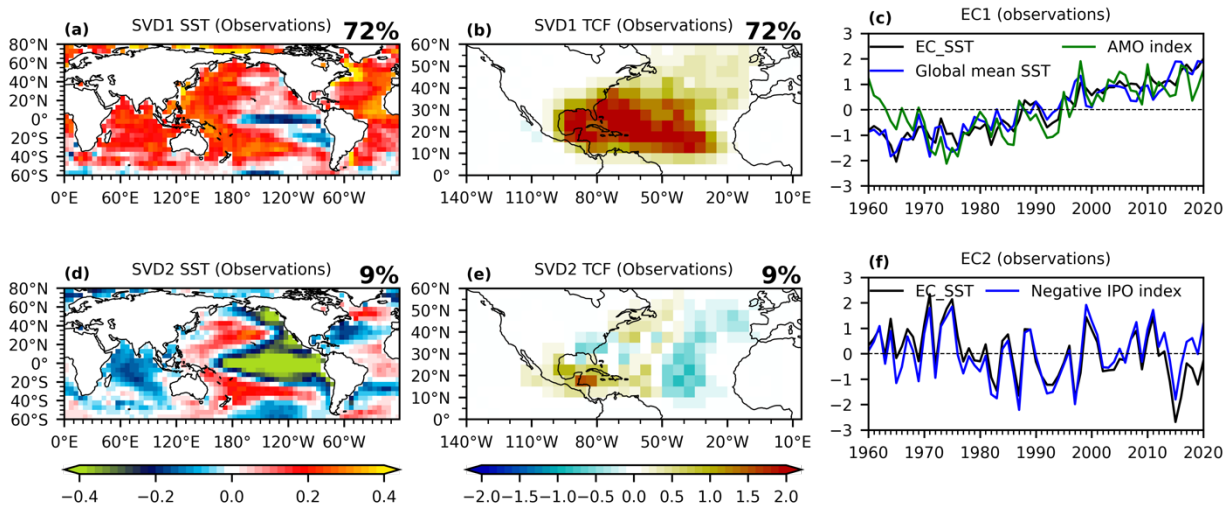

Supplementary Figure 2. Global SVD using global SST and TCF observation in North Altantic for the period 1960-2020. (a, b) The first SVD mode associated with (a) SST and (b) TCF. (c) Time series showing the expansion coefficient (EC) for the first SVD mode, overlaid with the global mean SST change and AMO index. The top-right corner of (a) and (b) displays the squared covariance fraction (SCF) for the first SVD mode. (d-f) Following the format of (a-c) but showing the second SVD mode. In (f), the time series of global mean SST and AMO index is substituted with the time series of inverted IPO index.

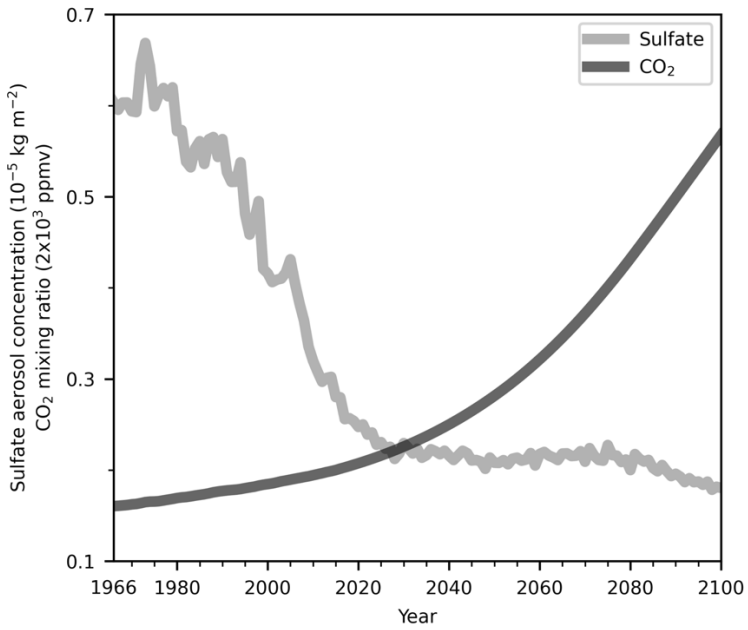

Supplementary Figure 3. Column-accumulated sulfate (light) averaged within the area of 20-70°N and 100°W-60°E (i.e., over Europe and the United States only), and CO_2 mixing ratio (dark). Historical records and SSP5-85 are combined.

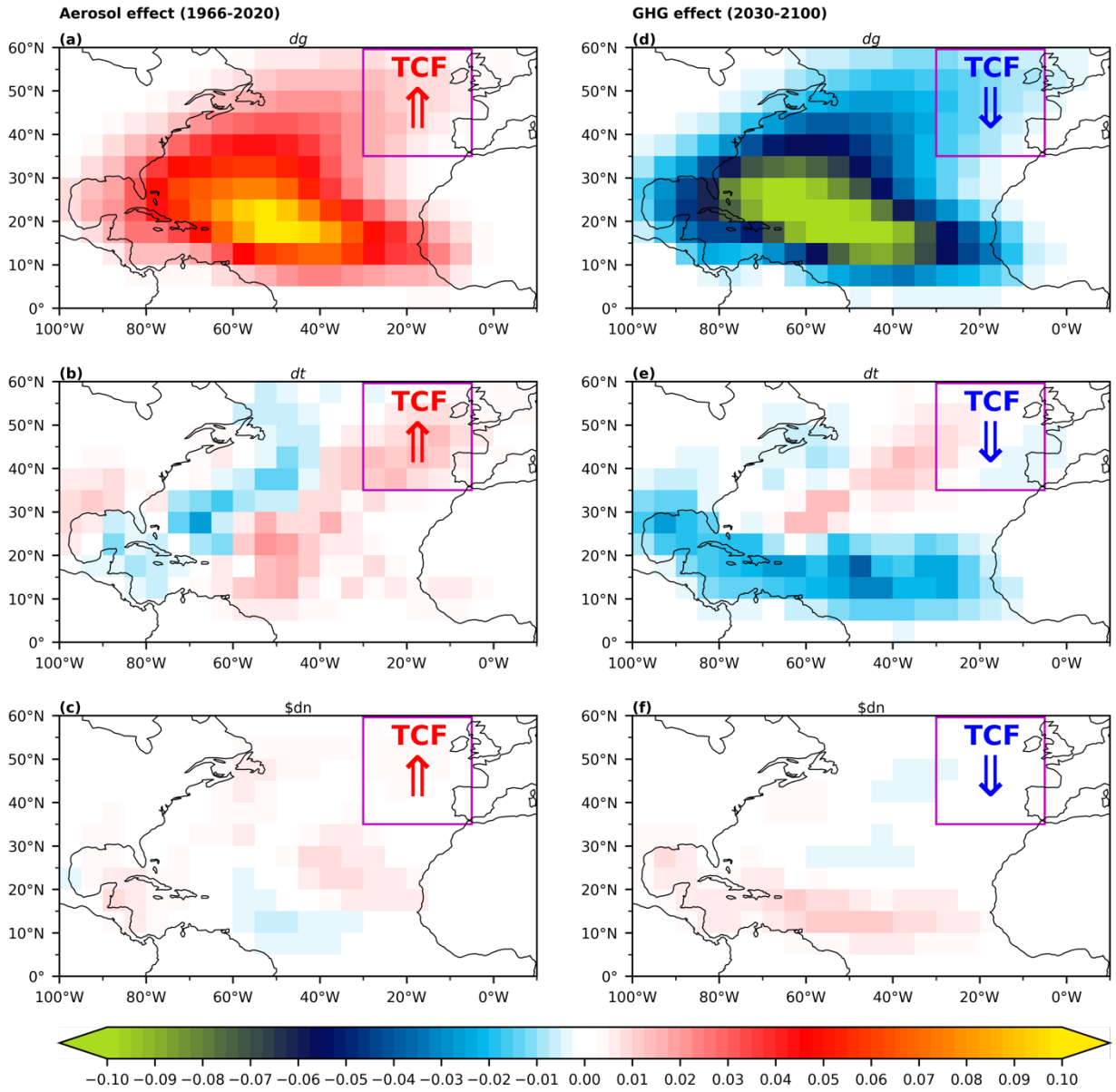

Supplementary Figure 4. The "Total Analysis" breaking down the overall change in TCF, as shown in Figures 2a and 2f, into the contributions by (a,d) genesis change, (b,e) track change, and (c,f) nonlinear combination of the genesis and track. The magenta box shows the same area near Western Europe as identified in Figure 1a. The overall TCF changes in the magenta box under aerosol (1966-2020) or GHG (2030-2100, SSP5-85) effects as shown in Figures 2a and 2f are denoted by "TCF increasing" and "TCF decreasing", respectively, in the magenta box.

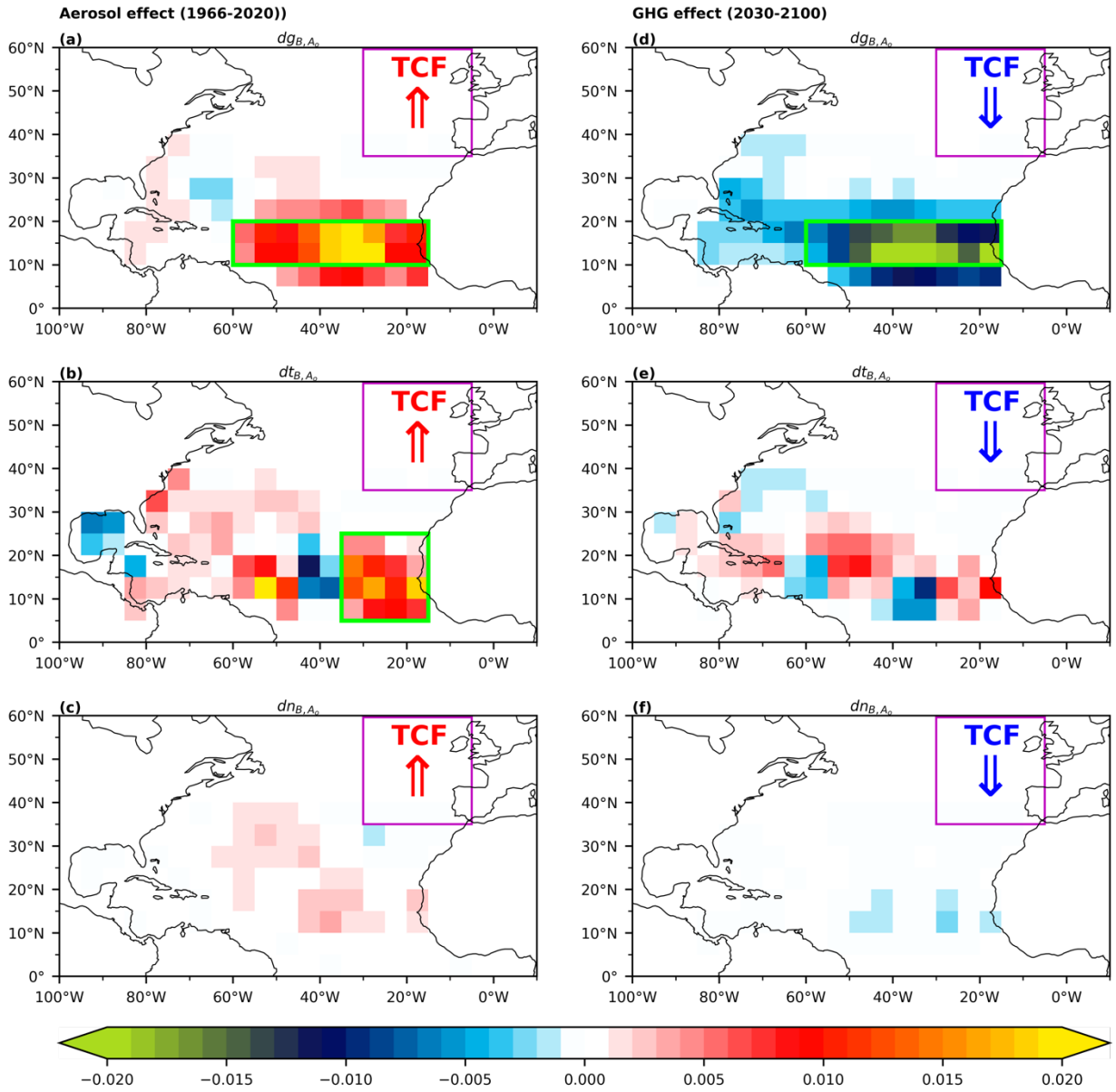

Supplementary Figure 5. The "Origin Analysis". The contribution of each grid to the total TCF change (df) in the magenta box due to genesis change (dg_{B,A_o}), TC track change (dt_{B,A_o}), and nonlinear combination of genesis and track changes (dn_{B,A_o}).

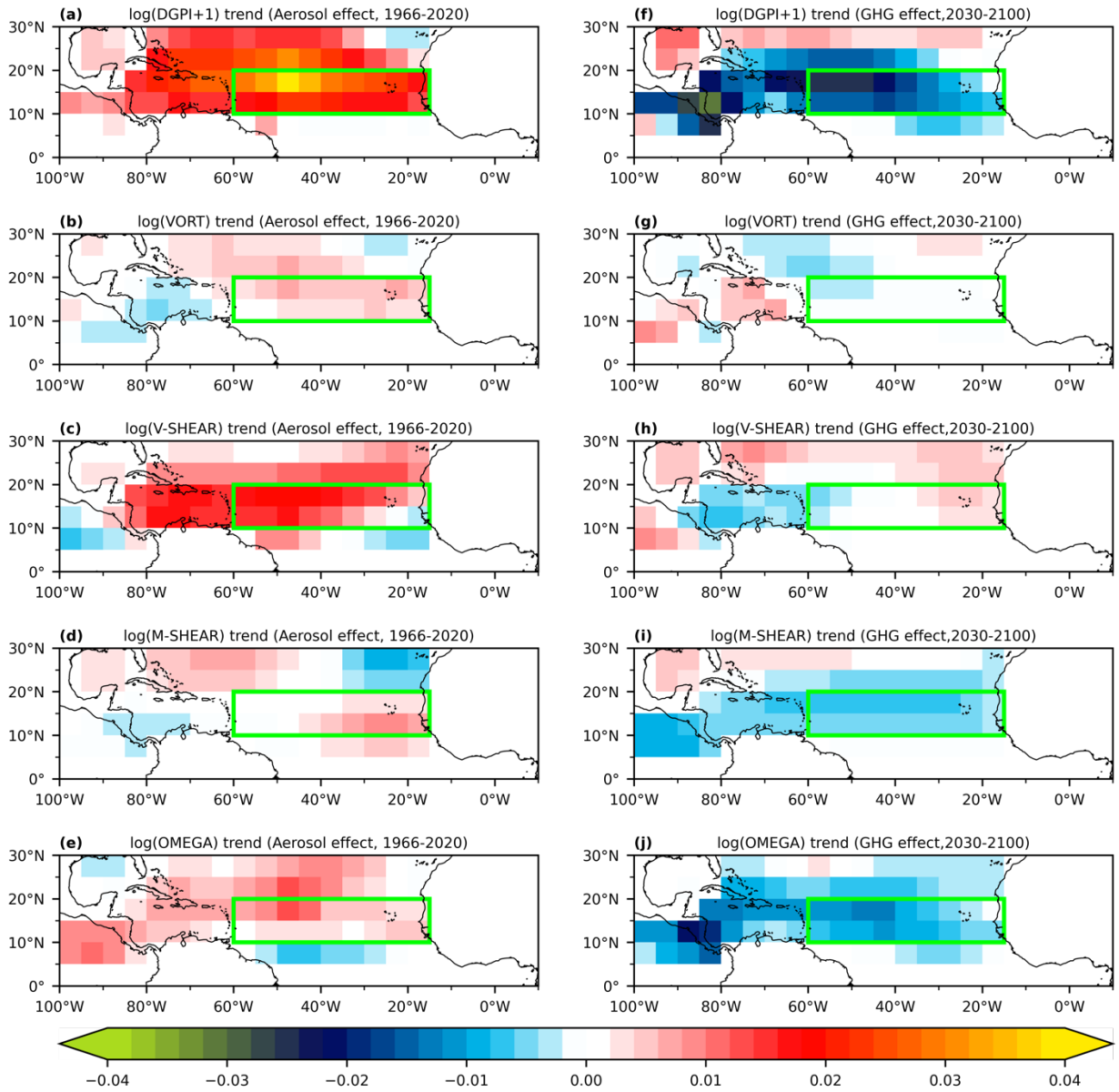

Supplementary Figure 6. DGPI trend decomposition (a-e) under the aerosol effect for 1966-2020 and (f-j) under the GHG effect for 2030-2100 (SSP5-85). The trends are based on the mean change during the main TC seasons (August-October).

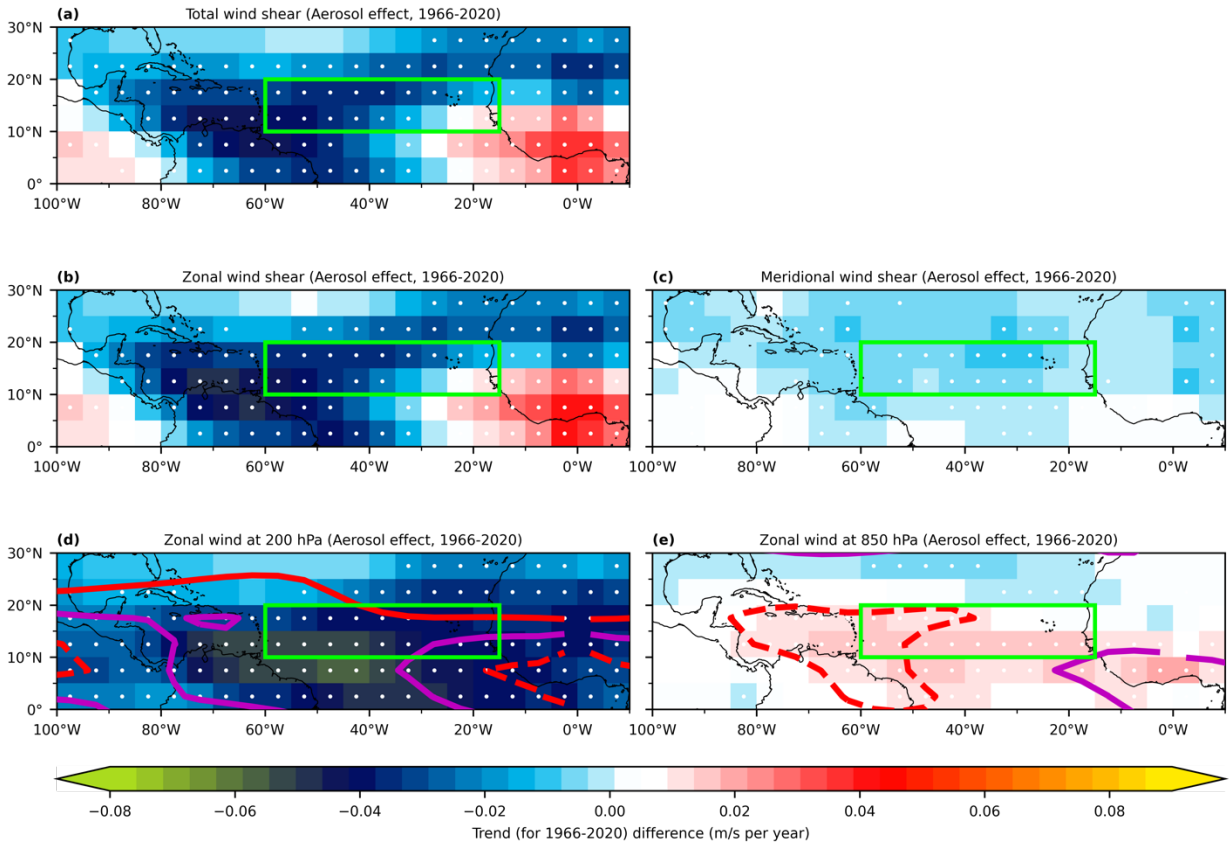

Supplementary Figure 7. Ensemble-mean trend difference under the anthropogenic aerosol effect of (a) total vertical wind shear, (b) zonal wind shear, (c) meridional wind shear, (d) zonal wind at 200 hPa, and (e) zonal wind at 850 hPa. The ensemble-mean climatology of -5, 0 and 5 m s^{-1} zonal wind speed contours are denoted by the dashed red, solid magenta and solid red lines, respectively. The white dot shows a significant trend difference at a 90% confidence interval. The trends are based on the mean change in each year of 1966-2020 during the main TC seasons only (August-October).

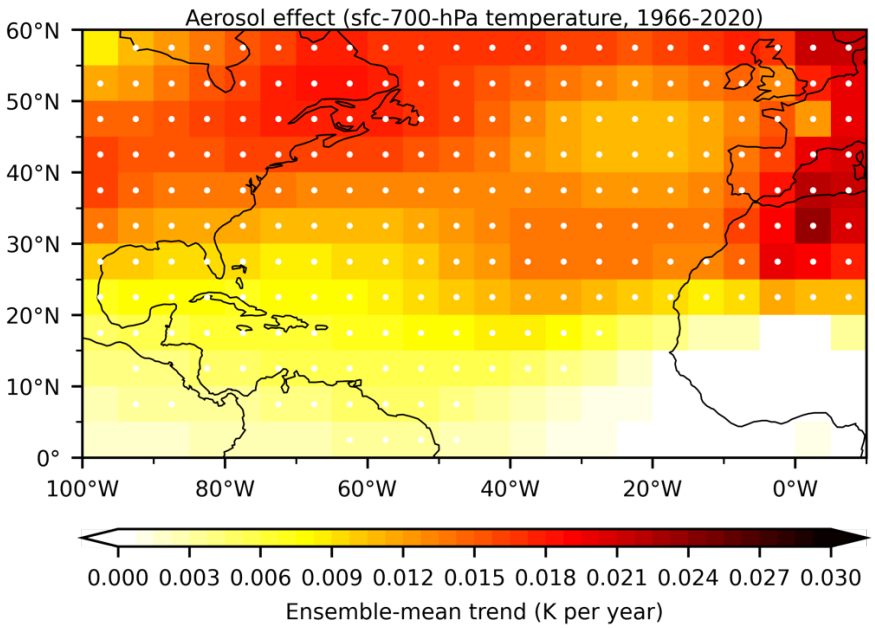

Supplementary Figure 8. Ensemble-mean trend of lower tropospheric temperature (surface-to-700-hPa) for 1966-2020 under the anthropogenic aerosol effect. The white dot shows a significant trend difference at a 90% confidence interval. The trends are based on the mean change in each year of 1966-2020 during the main TC seasons only (August-October).

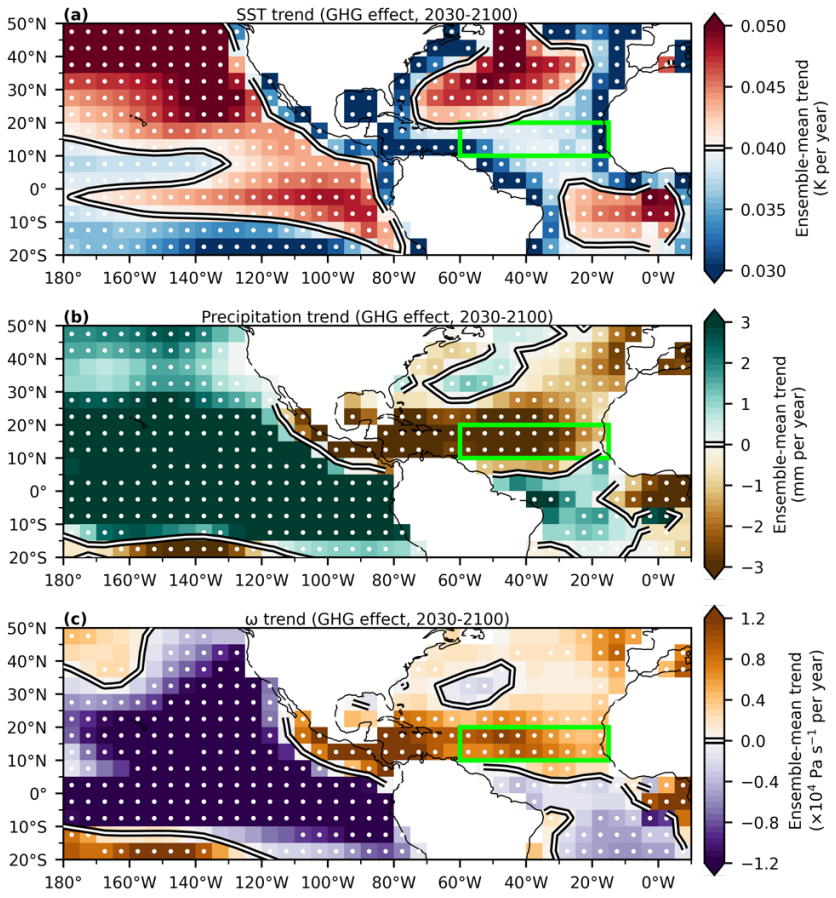

Supplementary Figure 9. Ensemble-mean trend of (a) SST, (b) precipitation and (c) ω for 2030-2100 under the anthropogenic GHG effect. The white dot shows a significant trend difference at a 90% confidence interval. The trends are based on the mean change in each year of 1966-2020 during the main TC seasons only (August-October).

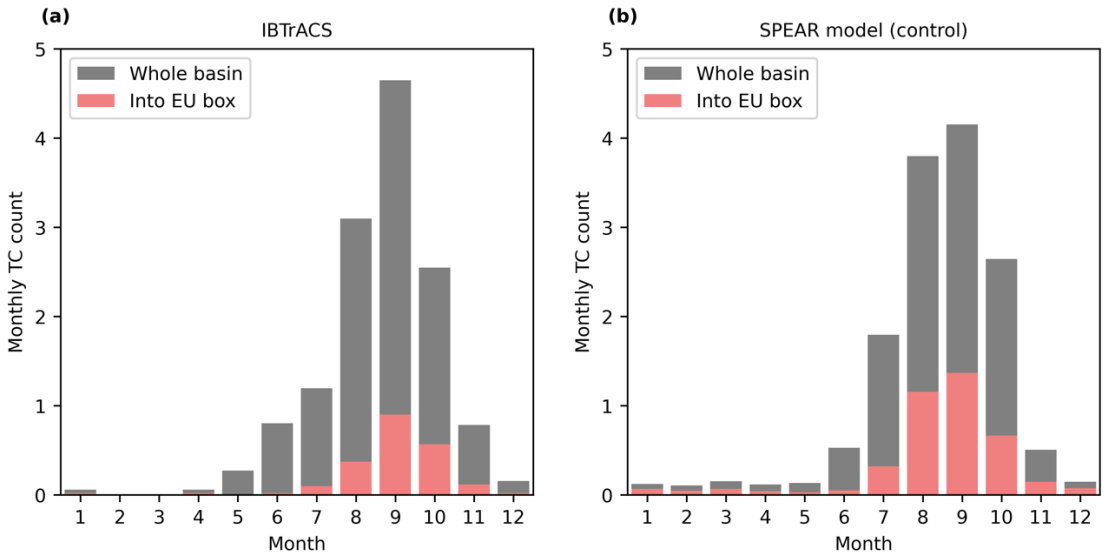

Supplementary Figure 11. Seasonality of monthly total TC count in the North Atlantic basin (gray bars) and in the magenta box near Western Europe (pink bars) as shown in Figure 1a. (a) IBTrACS for 1966-2020. (b) SPEAR model ensemble-mean of the control run from model year 1000 to 3000.